BIOPHYSICS

Flies land upside down on a ceiling using rapid visually mediated rotational maneuvers

Pan Liu[1], Sanjay P. Sane[2], Jean-Michel Mongeau[1], Jianguo Zhao[3], Bo Cheng[1]*

Flies and other insects routinely land upside down on a ceiling. These inverted landing maneuvers are among the most remarkable aerobatic feats, yet the full range of these behaviors and their underlying sensorimotor processes remain largely unknown. Here, we report that successful inverted landing in flies involves a serial sequence of well-coordinated behavioral modules, consisting of an initial upward acceleration followed by rapid body rotation and leg extension, before terminating with a leg-assisted body swing pivoted around legs firmly attached to the ceiling. Statistical analyses suggest that rotational maneuvers are triggered when flies' relative retinal expansion velocity reaches a threshold. Also, flies exhibit highly variable pitch and roll rates, which are strongly correlated to and likely mediated by multiple sensory cues. When flying with higher forward or lower upward velocities, flies decrease the pitch rate but increase the degree of leg-assisted swing, thereby leveraging the transfer of body linear momentum.

INTRODUCTION

Flies are agile small fliers that routinely perform a wide variety of aerodynamic feats (*1*–*3*). Among these, landing upside down on a ceiling (i.e., inverted landing) (*4*) is arguably among the most difficult and least understood aerobatic maneuver. Inverted landing requires small fliers, whether robotic or biological, to rapidly coordinate distance, velocity, and body orientation, using simple but fast sensorimotor processing. Smaller fliers also rely more on passive mechanical and structural processes, for their favored size dependency (*5*, *6*), to partially alleviate the demand on sensing and computation. In particular, flies landing on vertical (*7*, *8*) or inverted (*4*, *9*, *10*) surfaces use their extended legs to assist a body swing, or a "cartwheel," to align their body with the landing surface. This process relies heavily on the adhesion from cushion-like pads on their feet (called pulvilli) (*11*), which ensures a firm grip, and the viscoelasticity of the compliant leg joints, which damps out impact upon contact (*7*, *9*). Visual computation then acts in concert with these mechanical adaptations and initiates the leg extension (*12*) that is commonly considered stereotyped (*13*). Thus, for a successful landing, flies and other insects may not need to actively adjust their body orientation (via a controlled body rotational maneuver) immediately before the touchdown (i.e., when tarsi touch the substrate).

However, past research on inverted landing suggests that flies sometimes exhibit and, therefore, are at least capable of generating rapid rotational maneuvers immediately before touchdown. For example, Hyzer (*4*) described that flies (*Musca domestica*) occasionally performed a "half-roll" body rotation before touching the ceiling with their ipsilateral feet; this was followed by a lateral leg-assisted body swing that brought the other four feet into contact with the ceiling. Recent observations on inverted landing (*9*) showed that flies (*M. domestica*) actively pitched up their body before contacting the ceiling, sometimes using a combination of roll, pitch, and yaw body rotation. These observations, albeit limited, suggest that rapid body rotational maneuver may be a critical yet versatile component of the inverted landing behaviors. Moreover, their patterns are also likely mediated by visual and other sensory processes immediately before the touchdown.

In this study, we investigated the inverted landing behaviors of blue bottle flies (*Calliphora vomitoria*) in a flight chamber using high-speed videography (Fig. 1A). The kinematics of the flies' body and wing were extracted through digitization of anatomical landmarks (Fig. 1, B and C). First, we describe the sequential behavioral modules of the inverted landing, along with the kinematic variations in successful landings, and differences between successful and failed landings. We next show that the rotational maneuvers, occurring immediately before the touchdown, are triggered by retinal expansion. Their peak pitch and roll rates are correlated with and therefore likely mediated by multiple sensory cues. Last, we quantify the changes of wing kinematic patterns that generate these rotational maneuvers. Our study provides critical insights on inverted landing behaviors and the underlying biomechanical, sensory, and neural processes. It also points to possible mechanisms that can enable small-animal or robotic systems with limited computational resources to generate fast yet complex behaviors.

RESULTS

Behavioral modules in successful inverted landing

Fruit flies (*Drosophila*) land on vertical surfaces by continuous deceleration with negligible body rotation before the touchdown (*8*, *14*). In contrast, blue bottle flies (*Calliphora*) landing on a ceiling exhibited a sequence of four behavioral modules—started with an upward acceleration, followed by a rapid body rotational maneuver and leg extension, and ended with a leg-assisted body swing with forelegs firmly planted on the ceiling, thereby orienting the fly's body ventral side up (i.e., inverted) (Fig. 1 and fig. S3, Aii and Bii). The process from the start of the body rotation to the ventral side up landing lasted approximately four to eight wingbeats in all the successful landings (n = 18; table S1) (average wingbeat frequency, 172.7 ± 7.7 Hz).

In successful inverted landings, we observed substantial kinematic variations in the axes of rotation and the magnitude of rotational maneuvers, as well as in the degree of leg-assisted body swing. Thus, flies used a wide range of maneuvers when landing on a ceiling, which we categorized into pitch dominated, roll dominated, pitch and roll combined, and longitudinal or lateral body swing dominated (movie S1 to S5 and table S1). Examples of three typical sequences are shown

[1]Department of Mechanical Engineering, Pennsylvania State University, University Park, PA 16802, USA. [2]National Centre for Biological Sciences (NCBS), Tata Institute of Fundamental Research, GKVK Campus, Bellary Road, Bangalore 560065, India. [3]Department of Mechanical Engineering, Colorado State University, Fort Collins, CO 80523, USA.
*Corresponding author. Email: buc10@psu.edu

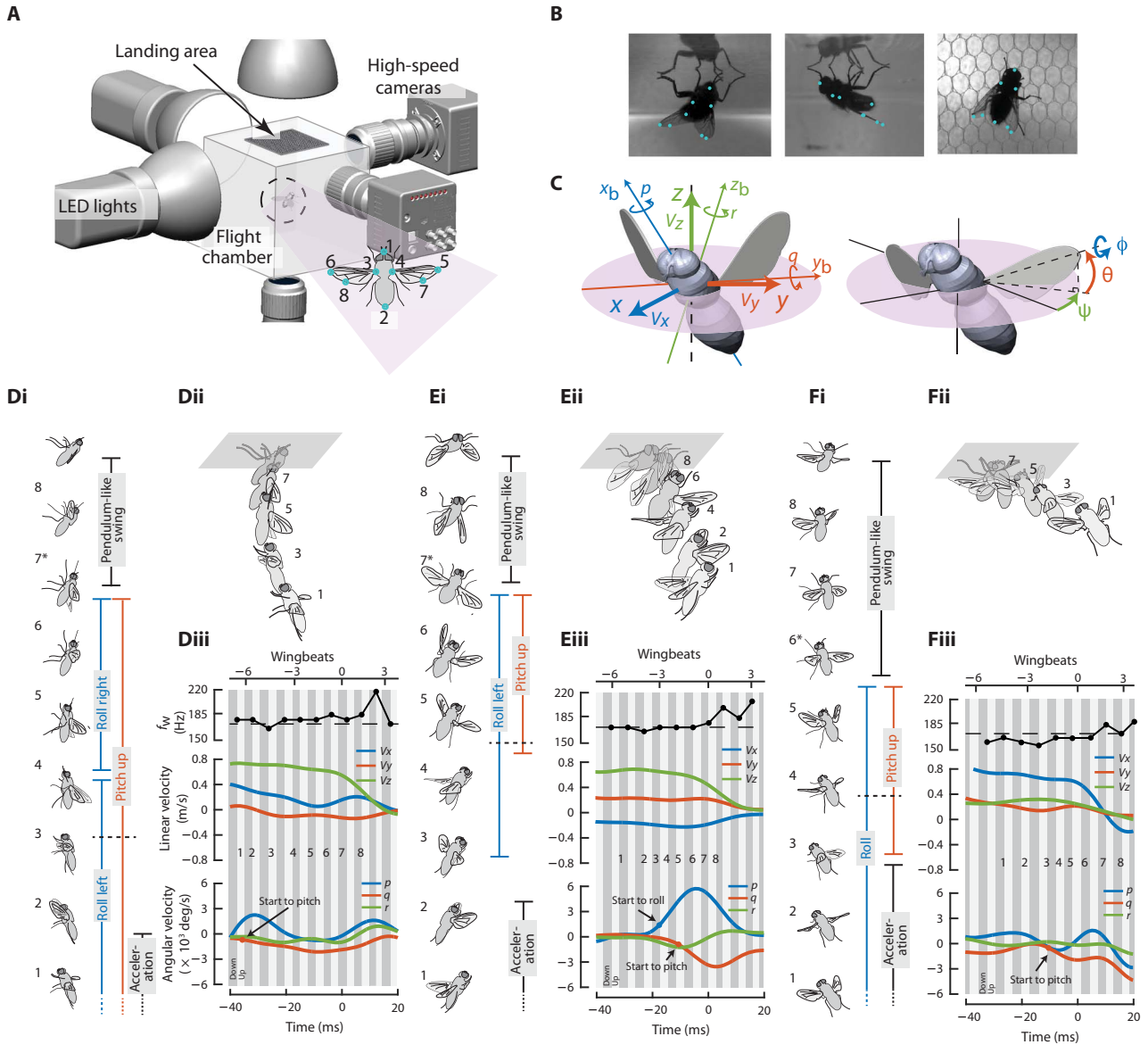

Fig. 1. Experimental setup, kinematic definitions, and some examples of diverse inverted landing sequences. (**A**) Landing maneuvers of flies are captured by three high-speed cameras operating at 5000 frames/s with exposure of 1/25,600 s. The landing area (10 cm by 10 cm) is located at the center of the ceiling of the flight chamber (20 cm by 20 cm by 20 cm) and is covered by mesh patterns to enhance visual contrast. (**B**) Anatomical landmarks of the flies from the captured images are digitized, from which we determine the body and wing kinematics according to the coordinate systems and kinematic angles defined in (C). (**C**) Body rotation is defined with respect to the body-fixed frame $\mathcal{F}_b = \{x_b, y_b, z_b\}$, where angular velocity is represented by roll p, pitch q, and yaw r rates. Body translational velocity relative to the ceiling is calculated with respect to the yaw-aligned global frame $\mathcal{F} = \{x, y, z\}$, which is obtained via rotating the global frame by the fly's yaw angle. The translational velocity is represented by forward/aft V_x, lateral V_y, and vertical V_z components. Wing kinematics are described by three Euler angles: stroke ψ, deviation θ, and rotation ϕ. The inverted landing behaviors are exemplified by those with rapid rotational maneuvers primarily about (**D**) pitch or (**E**) roll axes, and (**F**) those with a large leg-assisted body swing. (i) Sketches of flight sequences are separated spatially to make each instance visible. The instant when flies start to extend forelegs is denoted by the horizontal black dash line. (ii) Sketches of flight sequences are shown in their actual relative spatial locations. (iii) The time traces of wingbeat frequency f_w; body translational velocities V_x, V_y, and V_z; and body angular velocities p, q, and r. The time 0 represents the instant when a fly's leg first touches the ceiling, which is also indicated by the asterisk in (i). Black dashed lines in the subplots of f_w denote the average wingbeat frequency of the reference wing kinematics (173 Hz), measured during the upward-acceleration phase prior to the rotational maneuvers. The time instants starting to pitch or roll are identified separately as the instants when the pitch or roll rate reaches one-fourth of the corresponding peak rate. In comparison to (D) and (E), where flies maintain high upward velocities V_z (~0.8 m/s) and reach nearly ventral side up orientations by actively generating rapid pitch or roll maneuvers, the landing maneuver exemplified in (F) is characterized with large forward velocity V_x and negligible body rotational maneuver before forelegs touchdown. (Photo credit: Bo Cheng, Pennsylvania State University.)

in Fig. 1 (D to F), illustrating parts of this variation. In the first two examples, flies used rapid rotational maneuvers primarily about pitch (Fig. 1D and movie S1) or roll (Fig. 1E and movie S2), which oriented their body to a nearly inverted orientation before touchdown. Leg extension occurred slightly after the start of the rotational maneuvers (horizontal black dashed lines, Fig. 1, Di and Ei), and the body swinging phase followed after legs were planted on the substrate. Notably, the average peak angular rate of the rotational maneuvers reached approximately

4000°/s (fig. S3, Av and Bv) and could be as high as 6000°/s (Fig. 1Eiii), greater than those reported in the escape maneuvers of fruit flies (*1*) and hummingbirds (*15*). In the third example, flies relied almost entirely on the leg-assisted body swing to reorient and landed with negligible rotational maneuver (Fig. 1F and movie S3), similar to previously reported landing on vertical surfaces (*4*, *8*). Thus, compared with the first two, this landing strategy likely leveraged more of the mechanical and structural processes (e.g., adhesion due to pulvilli or damping due to viscoelasticity of leg) (*16*), which assisted the transfer of the body's linear momentum to rotational momentum.

Kinematic differences between successful and failed landings

We observed both successful and failed landings. A subset of flies landed in a smooth and coordinated fashion (successful landings), whereas others failed to land properly and collided head-on upon approach (failed landings). In successful landings, the four behavioral modules collectively led to a proper combination of body inversion and linear velocity with properly positioned legs prior to touchdown.

To quantify how well a fly's body was oriented, we calculated the degree of inversion (DoI), which measures the degree to which the fly's body is aligned with respect to a fully inverted orientation before touchdown (see Materials and Methods). DoI ranges from 0, representing no body inversion (or ventral-side down), to 1, representing full body inversion (or ventral-side up). In successful landings, the DoI increased with vertical velocity (Fig. 2A) but decreased with the forward velocity (Fig. 2B). This indicated that flies needed to be more inverted when their upward velocity was greater or when their horizontal velocity was lower. In most failed landings (total $N = 15$ analyzed; table S1), the flies were insufficiently inverted before touchdown, as compared with successful landings (Fig. 2). The failure in these landings can be attributed to delayed or minor body rotation prior to touchdown (Supplementary Materials). Consequently, these flies could not properly land on the ceiling but instead collided head-on. Notably, flies also failed at landing due to early rotation (see movie 7), as the early inversion led to insufficient vertical velocity to reach the ceiling ("+" in Fig. 2). Last, in some failed landings, flies had similar inversion to that of successful landings, but failed regardless. This happened due to delayed leg extension, which resulted in an improperly positioned leg to have the tarsi firmly planted on the substrate (see movie 8).

Yet, even after failed attempts, flies could still recover and land, using groping landing ($n = 24$; table S1). In this type of inverted landing, flies hover or fly at low vertical speed underneath the ceiling (Fig. 2), then they grope for the ceiling using their forelegs, and with a firm grip on the substrate, swing their body up to land (movie S6).

The kinematic complexities and variations in inverted landings indicate that they may involve more diverse neural processes than those reported for triggering leg extension and deceleration (*8*, *12*, *14*). In particular, the rotational maneuver with variable pitch and roll for a proper inversion was the major determining factor for success. Thus, in addition to being triggered, it is likely that the rotational maneuvers were mediated by sensory cues in a short period immediately before touchdown. We next examined the potential sensory cues and their roles in triggering and mediating the rotational maneuvers, based on the statistical analyses of the kinematic data.

Triggering of rotational maneuvers

We first describe the putative visual cues that flies could sense as they approach the ceiling with three components of linear velocity (vertical V_z, fore/aft V_x, and lateral V_y; Fig. 1C). Note that our study does not

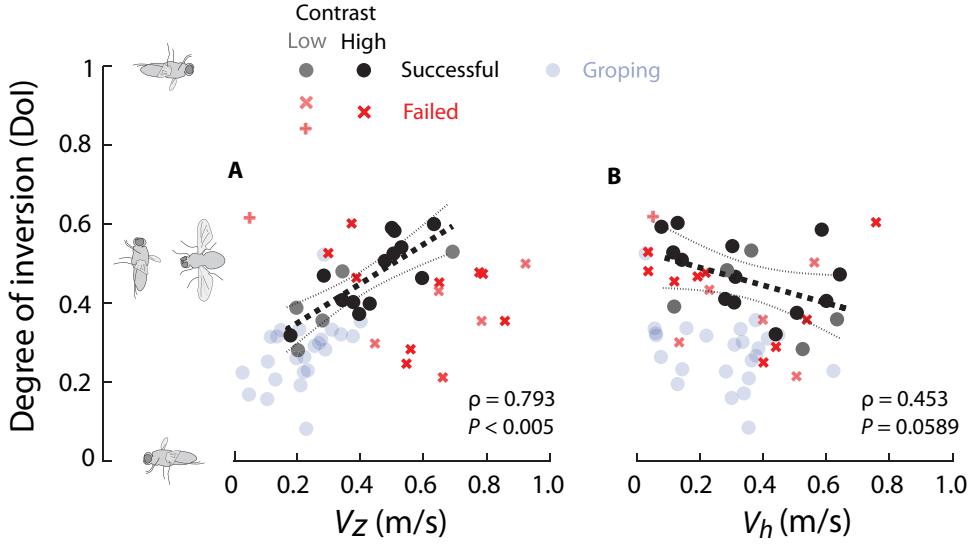

Fig. 2. DoI of the flies' body depended on the vertical and horizontal velocity components shortly before the feet touchdown in successful landing. For successful, groping, and failed landing cases, the DoI of flies' body are plotted against the vertical (V_z) and horizontal (V_h) components of flies' body linear velocity one wingbeat before the feet touchdown. Successful landing cases are marked in black, failed landing in red, and groping landing in light blue. The failed landing cases due to low body inversion and early body rotation are marked as "×" and "+," respectively. (**A**) DoI versus V_z and (**B**) DoI versus V_h. The highest V_z observed among successful landings is approximately 0.7 m/s. DoI ranges from 0, representing no body inversion (or ventral side down), to 1, representing full body inversion (or ventral side up). DoI increases with V_z but decreases with V_h in successful landing cases. For successful landings, the linear regressions between DoI and V_z, and DoI and V_h are shown with the Pearson's linear correlation coefficient ρ and P value; the 95% confidence intervals are also shown. In general, failed landing cases have lower DoI and higher V_z than the successful landing. Groping landing cases have relatively low DoI and low vertical velocity. The successful landing cases for low- and high-contrast landing areas are also differentiated.

consider feature-related triggering (e.g., object retinal location) (*8*), because, ideally, the use of uniform mesh grids should generate coherent motion over the entire retina when the fly is sufficiently close to the ceiling. Previous work on insect visual control (*8*, *14*, *17*) emphasized the importance of three types of visual cues. First is the relative retinal expansion velocity (RREV) due to looming stimuli (Fig. 3), which can be calculated as the ratio of a target's expansion rate to its size on the fly retina during upward translation (V_z). RREV also corresponds to the reciprocal of a physical variable called time to collision τ, which represents the time to collision, assuming constant velocity (*14*). RREV is considered an important perceptual cue that controls the approaching velocity during landing or obstacle avoidance (*18*, *19*). Second is the relative fore/aft angular velocity (or translational optic flow) of the ceiling on the fly retina (ω_y) (Fig. 4Ai). These visual cues result from the body fore/aft translation (V_x) and were found previously to control the grazing landing on horizontal surfaces (*17*). Third is the relative lateral angular velocity (or translational optic flow) of the ceiling ω_x on the fly retina (Fig. 4Bi), resulting from lateral translation (V_y). We calculated the time traces of these three visual cues in both the yaw-aligned global frame and the retina-fixed frame (fig. S4) using kinematic variables according to their mathematical relationships (fig. S1). All three visual cues could be calculated directly from the optic flow [see Supplementary Materials and (*19*)].

We assumed that the rotational maneuvers were triggered after a fixed time delay when the triggering visual cue reached a threshold (*14*). This is arguably the most parsimonious predictive model for the triggering and enabled us to test whether the above visual cues are related to the onset of the rotational maneuvers as described below.

We calculated the time traces of the coefficient of variance (CV) for each visual cue using trials in which flies landed successfully in their first attempt on a high-contrast landing area (table S1). The results for the RREV are shown in Fig. 3, while the complete results are shown in figs. S4 and S5 (Supplementary Materials). The CV measures the dispersion of a variable defined by the ratio of its SD and mean. The triggering of the pitch and roll motion was analyzed separately by aligning data from different landing trials at either the start of the pitch or roll. If the rotational maneuvers were triggered after some time delay when a visual cue reached a threshold value, the CV of this visual cue should be at its minimum. In addition, it should be lower than those of other nontriggering visual cues (*14*), i.e., the triggering visual cue should have the least dispersion (see Materials and Methods). For example, in a previous study on the triggering of linear deceleration in houseflies (*Musca domestica* L.) landing on vertical posts (*14*), the CV of the RREV is approximately 30%, lower than the other variables. Here, among the three visual cues tested, the RREV in the yaw-aligned global frame had the least CV for triggering either pitch (15%) or roll (25%) rotations (Fig. 3B), whereas the CV of the other two visual cues were significantly larger (figs. S4, A to C, and S5, A to C). This indicated that RREV was the primary visual cue triggering rotational maneuvers in inverted landing, similar to the triggering of deceleration for landing on vertical posts. Note that the CV of distance between the fly and the ceiling was close to that of the RREV (figs. S4D and S5D); however, flies are thought to not be able to directly measure distance (*20*, *21*).

The CV of the RREV was minimum, approximately between 7 ms (ΔT_l) and 27 ms (ΔT_u) before the onset of rotational maneuvers (Fig. 3B), suggesting that the visual latency ΔT between the instant of perception and the onset of a maneuver was within this small range. Although the latency inferred from this analysis was smaller than estimated from other behavioral studies, e.g., in linear speed control (*22*) and escape maneuvers (*1*), it fell within the range of latency in a fly's visuomotor pathway (*23*, *24*). Last, the corresponding RREV threshold value (Fig. 3B) indicated that the critical time to collision, below which the rotational maneuver was likely to be triggered, was between 31 and 53 ms. This threshold is lower than the one previously identified for triggering the prelanding deceleration in houseflies landing on vertical posts, which was approximately 76 ms (*14*).

Sensory mediation of rotational maneuvering patterns

Rotational maneuvers were highly variable in terms of their roll and pitch rates, which in successful landing have led to a proper body

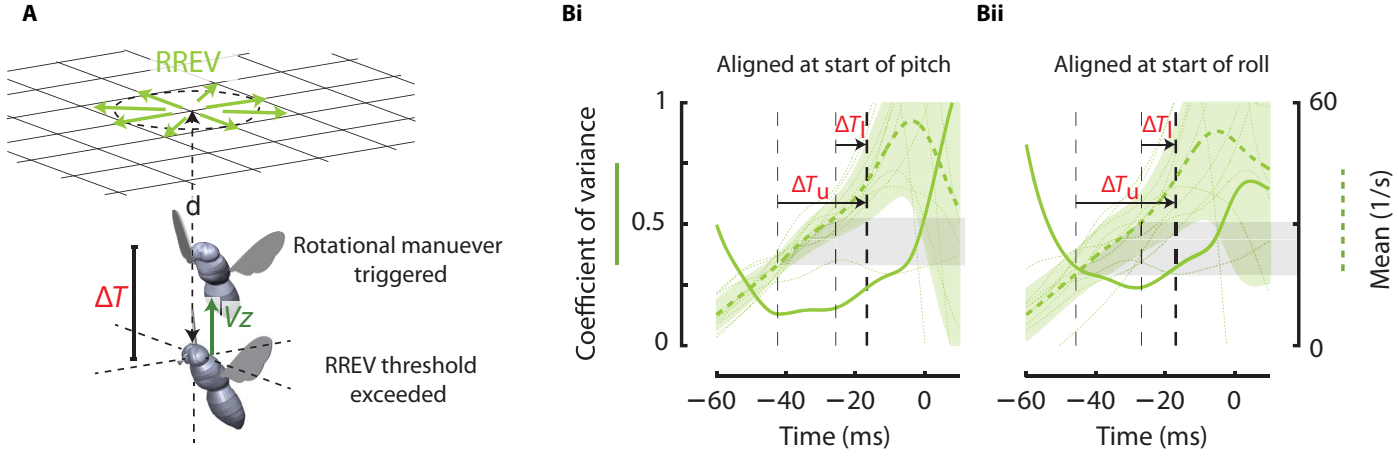

Fig. 3. The rotational maneuvers are triggered with short delays when RREV exceeds a threshold. (**A**) When a fly approaches the ceiling with velocity V_z, it perceives looming stimuli with increasing RREV on its retina. When RREV exceeds a threshold, the rotational maneuvers are triggered after a time delay ΔT. (**B**) Time traces of the coefficients of variation (CV) (thick solid green) and mean values (thick dashed green, the green shaded areas represent ±1 SD) of the RREV ($n = 10$). The time traces from the individual landing maneuvers (thin dotted green) are aligned at the instants when (Bi) the body pitch or (Bii) the body roll motion starts, as indicated by the thick black dashed lines. Time 0 indicates the averaged time instant when one of the fly's feet first touched the ceiling. The CV and mean values for the other estimated sensory cues are shown in figs. S4 and S5. To estimate the time delay ΔT, a time period when the CV of RREV reaches a low-value region is defined (between the two thin black dashed lines) (Supplementary Materials), the lower and upper bounds of which yield an upper bound (ΔT_u=27 ms) and a lower bound (ΔT_l = 7 ms) estimate of the time delay. The gray shaded areas represent the corresponding range of RREV threshold for triggering the rotational maneuver, which is between 19 and 32 rad/s, corresponding to time to collision between 53 and 31 ms, respectively.

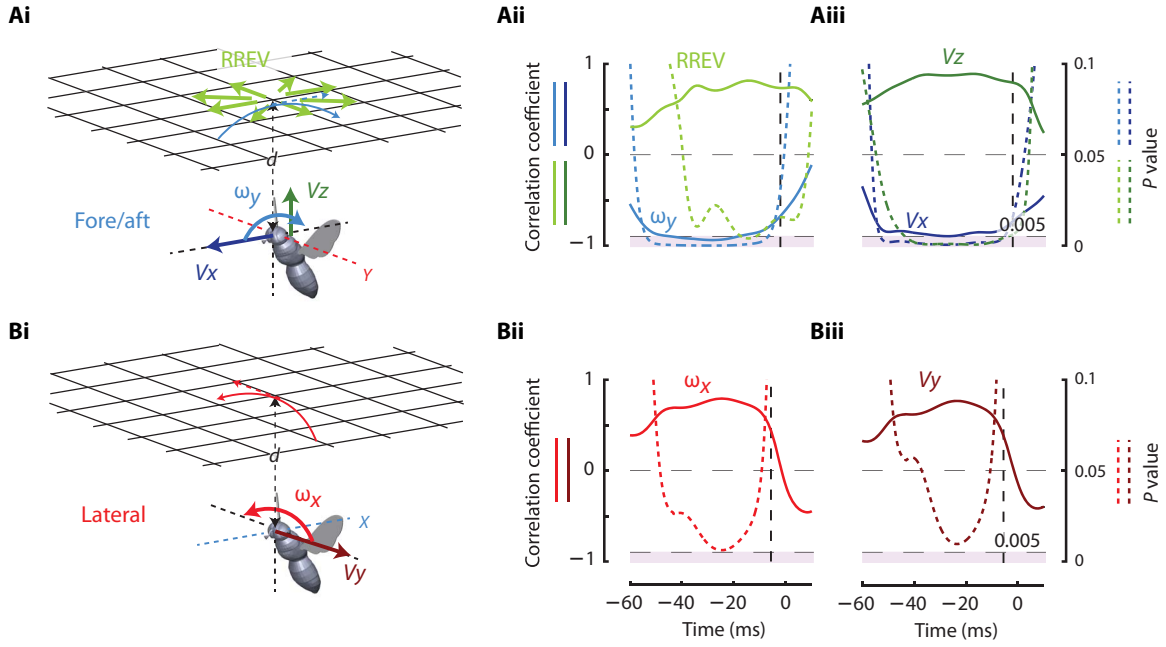

Fig. 4. The rotational maneuver patterns are correlated with multiple sensory cues perceived during inverted landing. (**Ai**) The fly's upward motion V_z results in RREV, and the fly's fore/aft motion V_x results in the ceiling rotating backward/forward on the fly's retina (ω_y about the *Y* axis). (**Bi**) Similarly, the fly's lateral motion V_y results in the ceiling rotating laterally (in an opposite direction) on the fly's retina (ω_x about the *X* axis). Among the successful landing trials, there exist strong correlations between peak pitch or roll rate and multiple sensory cues at different preceding time instants; the time traces of the corresponding correlation coefficients and the *P* value are shown for visual cues (Aii) ω_y, RREV and (Bii) ω_x, and mechanosensory cues (Aiii) V_x and V_z, and (Biii) V_y. As an example, fig. S8 shows the linear regressions between the peak pitch (or roll) rate with the visual cues at a particular preceding time instant (20 ms before the peak). The solid and dashed lines represent the Pearson's linear correlation coefficients and *P* value, respectively. The shaded areas indicate the region where $P \leq 0.005$. The peak pitch rate is positively correlated with RREV and V_z, and negatively correlated with ω_y and V_x. The peak roll rate is positively correlated with ω_x and V_y. All the time traces from different landing trials are aligned at the instant of peak pitch or roll rate, which is indicated by vertical black dashed lines. Time 0 indicates the averaged time instant when one of the fly's feet first touch the ceiling. The complete correlation results between the pitch (or roll) rate and the estimated sensory cues are shown in figs. S6 and S7 and table S2.

inversion according to the flies' body linear velocity (Fig. 2). This suggested that, in addition to the onset timings, the patterns of the rotational maneuvers were also mediated by sensory cues. Flies are known to use sensory cues to mediate rotational maneuvers via both feedforward and feedback pathways (*25*). The feedforward path issues spontaneous steering commands that produce large, transient wing motion changes, which determine the initial response magnitude of the maneuver (*25*, *26*). The feedback path mediates compensatory reaction (e.g., haltere-mediated feedback) that produces fine-scaled wing motion change, which determines the active damping and stabilizes the maneuver (*2*, *25*, *26*). Here, we identified the potential sensory cues and their roles in the feedforward mediation of the rotational maneuvers. This was achieved by identifying the correlations between the peak roll and pitch rates of the rotational maneuvers with the sensory cues perceived by flies prior to or slightly after the onset of the maneuvers. Note that these sensory cues were mainly dependent on the flies' body linear velocities shortly before the onset of rotational maneuvers, when body angular velocity was negligible.

Specifically, we evaluated correlations between the peak pitch and roll rates with a set of putative sensory cues at varying time instants prior to or slightly after the onset of rotational maneuvers (Fig. 4, and more details in figs. S6 and S7 and table S2). The correlations using the sensory cues 20 ms before the peak angular rates are shown in fig. S8 as an example. We used angular rates rather than angular acceleration because previous studies suggested that motor responses (i.e., wing kinematic control variables) were more strongly correlated with body angular rates due to the periodic and highly damped nature of flapping flight (*27*, *28*). The putative sensory cues included the three visual cues tested above for the triggering (RREV, ω_x, and ω_y) and the three components of body linear velocity (V_x, V_y, and V_z), which were likely perceived via mechanosensory modalities of flies (*29*). Linear regression analysis showed that, within a large time period prior to the onset of the maneuvers ($P < 0.05$, Student's *t* test), the peak pitch rate was positively correlated with RREV (Fig. 4Aii) and vertical velocity V_z (Fig. 4Aiii), but negatively correlated with fore/aft ceiling rotation ω_y (Fig. 4Aii) and fore-aft linear velocity V_x (Fig. 4Aiii). Similarly, peak roll rates were positively correlated with the lateral ceiling rotation ω_x (Fig. 4Bii) and lateral linear velocity V_y (Fig. 4Biii), also within a large period ($P < 0.05$, Student's *t* test) prior to or shortly after the onset of the maneuvers. The above correlation analysis supports the possibility of sensory mediation of rotational maneuver patterns, with pitch mediated by sensory cues encoding upward and fore/aft translation, and roll mediated by sensory cues encoding lateral translation.

The above correlation analysis also raised the possibility that flies modulate the magnitude of rotational maneuvers to exploit leg-assisted body swing, including transfer of linear to angular momentum. Specifically, flies exhibited a reduced pitch rate when forward linear momentum was high, as indicated by the negative correlation between peak pitch rate with sensory cues resulting from forward translation (visual ω_y or mechanosensory V_x). Thus, instead of active pitching, flies inverted their body by increasing the leg-assisted longitudinal body swing and the transfer of forward linear momentum to pitch angular

momentum (Fig. 1F). On the other hand, flies exhibited an increased roll rate when the lateral linear momentum was high, as indicated by the positive correlation between peak roll rate and sensory cues resulting from lateral translation (visual ω_x or mechanosensory V_y). This opposite correlation may result if flies need sufficiently large banking to raise their ipsilateral legs high enough to reach the ceiling for the leg-assisted body swings (middle legs cannot extend upward as high as forelegs without banking the fly's body). Thus, this strategy could also assist the execution of lateral body swings that transferred lateral linear momentum to roll angular momentum.

Wing kinematic patterns that produce pitch and roll

The execution of the rotational maneuvers requires sensorimotor transduction of sensory cues to motor outputs that help modulate wing motion to generate various aerodynamic forces and moments. We next examined the changes of wing motion responsible for generating pitch and roll during rotational maneuvers. The wing motion patterns underwent moderate changes that lie between those reported in fruit flies (*1*) and hummingbirds (*27*) during escape maneuvers. We observed the following changes. First are the bilaterally symmetric changes in wing spanwise rotation (Fig. 5, A and Ci) and bilaterally symmetric

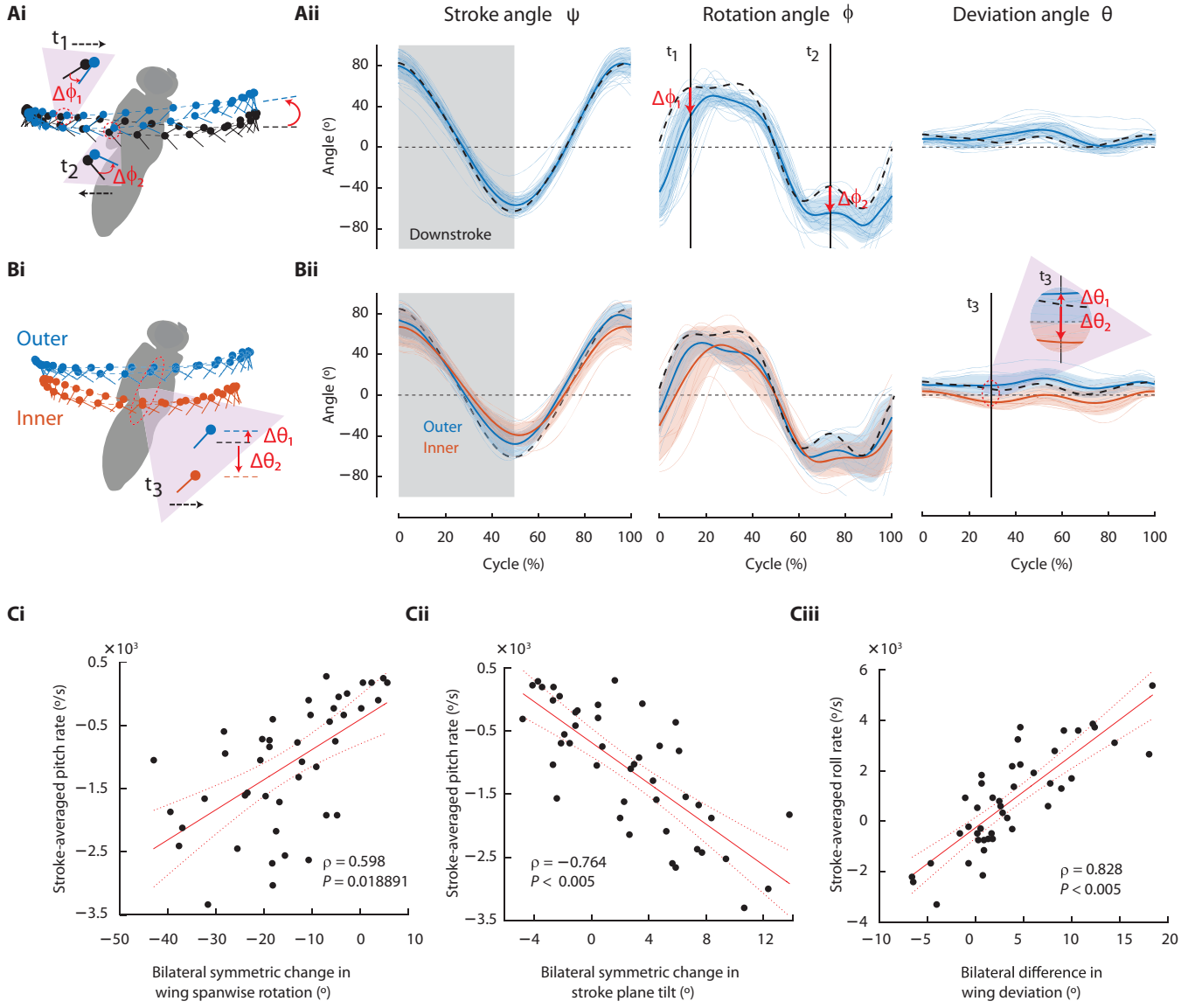

Fig. 5. The rotational maneuvers are generated by the modulation of wing kinematic patterns. (**Ai**) To generate nose-up pitch rotation, a fly tilts its stroke plane backward and shifts its mean wing spanwise rotation angle backward. (**Bi**) To generate roll rotation, a fly elevates the outer wing and lowers the inner wing, thereby tilting its stroke plane laterally toward the inner wing. Changes in the instantaneous wing kinematic patterns for generating pitch (Aii) and roll (Bii) within a time-normalized wingbeat cycle: stroke ψ, rotation ϕ, and deviation θ angles. The thick and thin solid lines represent the averaged and individual wing kinematics. The shaded areas represent ±1 SD. The dashed black lines represent the reference wing kinematics (see fig. S9). The linear regressions between stroke-averaged pitch/roll rates and the changes of wing kinematics are shown with the Pearson's linear correlation coefficient ρ and *P* value. The stroke-averaged pitch rate is strongly correlated with bilateral symmetric change in stroke plane tilt and wing spanwise rotation. The stroke-averaged roll rate is strongly correlated with bilateral asymmetric change in wing deviation (i.e., the lateral tilt of stroke plane).

changes in stroke plane angle (Fig. 5, A and Cii), which were both strongly correlated with the pitch rate (for example, to produce nose-up pitch, the fly tilted its stroke plane and shifted the mean rotation angle backward). Second are the bilateral differences in wing deviation (Fig. 5, B and Ciii), which were strongly correlated with the roll rate. The bilateral differences in wing deviation, which resulted in the lateral tilt of stroke plane, have also been observed in escape maneuvers in hummingbirds (*27*) and fruit flies (*1*). In addition, bilateral differences in wing stroke amplitude and mean wing rotation were observed and likely contributed to the roll. More details of the variables of wing motion changes and their correlations with body angular rates are provided in table S3. Despite the size and physiological differences, the variables of wing motion changes for generating pitch and roll during the inverted landing in flies closely resemble those of hummingbirds during escape maneuvers (*27*).

DISCUSSION

In summary, our results indicate that flies execute inverted landings by a well-coordinated sequence of behavioral modules (Fig. 6), including rapid rotational maneuvers and leg extension, followed by touchdown and a final leg-assisted body swing that brings all feet into contact with the ceiling. The rotational maneuvers were markedly more complex than previously reported in insects landing on surfaces of various orientations (*8*, *12*, *14*, *19*) in studies that mainly highlighted the importance of visually triggered leg extension or deceleration, rather than the rotational maneuvers, for successful landing.

Our results suggest that inverted landing may involve neural processes that not only compute the RREV that encodes time-to-collision

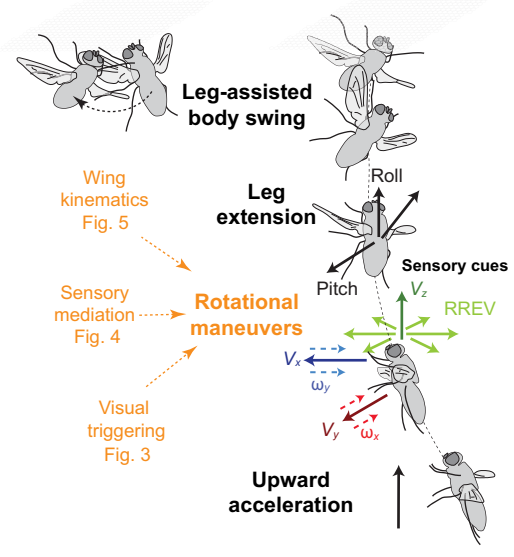

Fig. 6. Summary of visually mediated inverted landing. A fly landing on a ceiling starts with an initial (i) upward acceleration, followed by (ii) rapid rotational maneuvers and (iii) leg extension, and ends with a (iv) leg-assisted body swing with forelegs firmly attached on the ceiling. In successful landing, the rapid rotational maneuvers orient the fly to a proper inversion according its linear velocity. The rotational maneuvers are triggered when RREV exceeds a threshold and are likely mediated by multiple visual (ω_x, ω_y, and RREV) and/or mechanosensory (V_x, V_y, and V_z) cues. The complex behavioral modules observed, particularly the highly variable rotational maneuver, suggest that inverted landing likely involves multiple neural pathways, in addition to those reported earlier for leg extension in vertical landing.

information but also integrate it with other sensory cues that putatively encode multiaxis body linear translation (Fig. 6). Our analyses of the sensory mediation of rotational maneuver (Fig. 3) are entirely correlational at the current time and, as yet, do not establish a causal relationship between sensory cues and the observed maneuvers. However, they do suggest specific hypotheses about how multiple sensory cues could influence landing behavior and success. These data will guide future experiments with controlled manipulation of selected sensory cues from the landing surface, thereby to develop a more complete predictive model of inverted landing.

The rotational maneuvers in inverted landing appear to share a similar ballistic nature to the escape responses that initiate the flight (*30*). These maneuvers occurred shortly after startling the flies and immediately before the touchdown and exhibited remarkably high angular velocity. To our knowledge, the values we measured were the maximum reported in actively maneuvering flies. Escape responses in flies are mediated by the giant fiber (GF) that gives rise to fast motor program selection and timing (*30*); the GF also integrates angular expansion velocity and angular size cues and may therefore be responsible for extracting the RREV (*30*). Because both escape and landing are triggered by looming stimuli, it would be important to determine the extent to which these distinct behaviors share common neural pathways.

It can be hypothesized that the variability of the rotational maneuvers arose mainly from the passive flight dynamics in the absence of any sensory mediation, evolving from different initial flight states (*31*, *32*). However, our results do not support this hypothesis. Both computational (*32*, *33*) and experimental (*28*, *34*) results indicate that forward translational velocity induces a pitch-up moment, and the upward translational velocity induces negligible pitch moment in flying insects [see the estimation of stability derivatives (*35*–*39*)]. If the pitch rotation of the flies was mainly determined by the initial flight states via the dynamic processes, this would suggest a negative correlation between the upward velocity and pitch rate and weak correlation between the upward velocity and pitch rate, which contradict the above correlations (Fig. 4Aiii). Thus, we conclude that the correlations between the sensory cues that encoded body linear motion with the roll and pitch rates must result from sensorimotor processes, rather than the passive flight dynamics depending solely on the initial conditions.

In addition to the rotational maneuvers, leg-assisted body swings also exhibited considerable variability in its degree of excursion and the number and types of legs involved. The triggering of leg extension was consistently observed in all successful landings, the timing of which, however, did not follow the onset of rotational maneuvers (Fig. 2, D to F), which were almost absent in landings dominated by leg-assisted body swings (Fig. 2F). Whereas this suggests possible separate neural pathways for leg extension and rotational maneuvers, previous efforts on the neural circuits of landing focused primarily on how leg extension reflex is triggered (*13*, *40*, *41*). The use of legs also appeared to be multifunctional: They can be mainly used to absorb shock (or as a passive braking mechanism) with relatively small body swing (movie S1) or to assist the body swing with large rotation between legs and the body (movie S3). These results are consistent with other observations in houseflies that the leg extension response can be highly variable and depends on local cues such as surface orientation, whereas body deceleration occurs in a more stereotypic fashion (*9*). A recent study also shows that amplitude of the leg extension in *Drosophila* is correlated with the spike rate of two identified descending neuron types, suggesting more finely controlled landing responses (*42*). These observations suggest

that landing behaviors can be thought of as behavioral modules that are either reflexive and rigid or sensory driven and variable (*9*). Therefore, future efforts should focus on identifying the diverse neural mechanisms that trigger and mediate different behavioral modules for the fuller understanding of the neural control of landing.

In addition, because the wings continued to beat during the leg-assisted body swings and showed considerable kinematic changes compared with those prior to touchdown (e.g., movie S3), there was also likely an active, sensory-driven torque generation from the wings. The various aspects of the leg-assisted body swing, including leg extension kinematics, feet contact mechanics, and the aerodynamic forces/torque generation from the wings, should be analyzed in future studies.

Last, our results also suggested that, for small biological or robotic fliers with limited onboard sensing and computing capacity, orchestrating a successful landing hinges critically on the integration of computational (e.g., fast image processing algorithms and circuits) and mechanical (e.g., compliant landing gears or legs) processes. The key visual cues identified in this study can all be estimated from optic flow measurements with relatively low computation (*43*, *44*). They help to trigger and control both the body rotation and the leg extension; body rotation can ensure a proper inversion, where leg extension helps passively damp out the collision and assist in momentum transfer. Recent advances in codesigning algorithms and hardware may offer practical solutions for rapidly computing visual cues on miniature integrated circuit (*45*, *46*), and embedding soft materials into rigid ones can potentially generate compliant landing gears with programmable motions (*47*–*49*).

MATERIALS AND METHODS

Experimental setup and kinematic calculation

Using three high-speed cameras, we captured the behaviors of blue bottle flies (*C. vomitoria*) landing upside down on the ceiling in a flight chamber (Fig. 1A) at the end of flight bouts that were triggered by mechanical vibrations of the chamber. The ceiling, backlit by a light-emitting diode light, was covered by two types of mesh pattern to provide low- or high-visual contrasts. The kinematics of both flies' body and wings were extracted through digitization of anatomical landmarks (Fig. 1B), from which the wing and body principal axes and the corresponding kinematic angles, linear and angular velocities, were calculated (Fig. 1C) (*11*). More details on the experimental setup and kinematic extraction are given in the Supplementary Materials.

Definition of DoI

Here, we defined the DoI of a fly's body orientation shortly before the feet touchdown. Using equation S5 in the Supplementary Materials, we first calculated the magnitude of the geodesic $d_{\Delta R}^{\min}$ (i.e., the shortest distance or the smallest angle) (*50*) between two body orientations: (i) the fly's orientation one wingbeat before the touchdown and (ii) the fully inverted landing orientation. $d_{\Delta R}^{\min}$ ranged from π (having no inversion; i.e., ventral side down) to 0 (being completely inverted; i.e., ventral side up). The DoI was then defined as

$$\mathrm{DoI} = \frac{\pi - d_{\Delta R}^{\min}}{\pi} \quad (1)$$

where DoI = 1 when the fly is completely inverted (i.e., ventral side up), and DoI = 1 when there is no body inversion (i.e., ventral side down).

Calculation of visual cues from body kinematics

The time traces of three putative visual cues were estimated to identify the triggering and visual mediation mechanisms of the rotational maneuvers. The visual cues included the RREV, the relative ceiling fore/aft rotation (ω_y), and the relative ceiling lateral rotation (ω_x). These visual cues can be perceived by a fly from the image sequence projected on its retina without the direct perceptions of the distance or the body velocities. The time traces of these visual cues during the course of inverted landing can be estimated from the measured body kinematics. More details on the kinematic relationships between the visual cues and the body kinematics are given in the Supplementary Materials.

Visual cues in triggering the rotational maneuvers

To analyze how the rotational maneuvers in inverted landings are visually triggered, we calculated the time traces of the CV of three putative visual cues (RREV, ω_y, and ω_x) prior to landing. The CV is a measurement of the dispersion of a variable defined by the ratio of its SD and mean. Assuming that rotational maneuvers are triggered after some time delay when the triggering visual cue reached a threshold at a particular time instant, then the CV of this visual cue at this time instant should be lower than those at other time instants; in addition, the CV of the triggering visual should be lower than those of other nontriggering visual cues. In short, the CV of the triggering visual cue should reach a minimum prior to the triggering moment and be the lowest when compared with the CV of other nontriggering visual cues.

In this analysis, we investigated the triggering of pitch and roll separately. Take the pitch triggering as an example. First, the time traces of the visual cues from different landing trials were aligned at the instant of the start of the pitch. Next, the CV was calculated for each of the visual cues. To identify the triggering visual cue, we first defined a low-value region for the CV of each visual cue (between the two breakpoints that sandwich the low-value valley region of a CV curve), and the visual cue with the lowest minimal CV was identified as the triggering cue. The mean value of this visual cue over the minimum CV range was identified as the triggering threshold. In addition, the time delay in the triggering process due to the sensorimotor transduction can be also identified. Identifying the triggering mechanism for the roll was similar to those for the pitch, except that the time traces of the visual cues were now aligned at the instant of the start of roll.

Sensory cues in mediating the rotational maneuvers

To study whether and how the patterns of rotational maneuvers were mediated by sensory cues in a feedforward fashion after being triggered, we calculated the Pearson's linear correlations between the rotational kinematic features and the putative sensory cues that flies may receive at different time instants prior to or during the rotational maneuvers. The rotational kinematic features tested included the peak, average, and integral of the angular velocities (p, q, and r) of the rotational maneuvers. The putative sensory cues tested included the visual (RREV, ω_x, and ω_y) and mechanosensory cues (V_x, V_y, and V_z). After some preliminary testing and analysis, it was determined that the peak pitch and roll rates best represent the patterns of rotational maneuvers as they also had the strongest correlations with the sensory cues compared with other rotational kinematic features. Therefore, next we calculated the time traces of the correlations between the peak angular rates and the sensory cues at different time instants prior to the moment of peak angular rates. For example, to calculate the correlation between the peak pitch rate and the RREV, the time traces of the RREV from different landing trials were first aligned at the instant of peak pitch rate; then,

the time trace of the Pearson's linear correlations between the peak pitch rate and the RREV at varying time instants prior to the peak pitch rate was calculated.

Wing kinematics in generating rotational maneuvers

The recorded wing kinematics were represented by the stroke ψ, deviation θ, and rotation ϕ angles and parameterized using Fourier series. These wingbeats were classified into reference and pitch- or roll-generating ones based on their corresponding angular accelerations. More details are given in the Supplementary Materials. To investigate the changes of wing motion that produced the rotational maneuvers, the Pearson's linear correlations between the changes of wing kinematic variables and body angular velocity and accelerations were calculated. The changes of wing kinematic variables include bilateral symmetric and asymmetric changes of stroke angle, wing rotation and deviation, stroke plane tilt, and wingbeat frequency. In addition, the correlation with stroke-averaged upward acceleration was also calculated.

SUPPLEMENTARY MATERIALS

Supplementary material for this article is available at http://advances.sciencemag.org/cgi/content/full/5/10/eaax1877/DC1

Supplementary Materials and Methods

Fig. S1. Relationship between the visual cues and the fly's body translational kinematics.

Fig. S2. Sketches of flight sequences of two failed landing attempts and the corresponding kinematics.

Fig. S3. Time traces of body kinematics of landing maneuvers dominated by pitch and roll.

Fig. S4. The pitch rotation in inverted landings is triggered when RREV exceeds a threshold.

Fig. S5. The roll rotation in inverted landings is triggered when RREV exceeds a threshold.

Fig. S6. Correlations between visual or mechanosensory cues to the pitch rate of the rotational maneuvers.

Fig. S7. Correlations between visual or mechanosensory cues to the roll rate of the rotational maneuvers.

Fig. S8. Linear regressions between peak pitch (or roll) rate and sensory cues at an example time instant of 20 ms before the time instant of the peak pitch (or roll) rate.

Fig. S9. The wing kinematics that generate upward acceleration prior to rotational maneuvers are defined as the reference wing kinematics.

Table S1. Categorized landing trials.

Table S2. The Pearson's linear correlation coefficient and *P* value between body rotation variables and multiple sensory cues at an example time instant of 20 ms before peak of rotation rate.

Table S3. The Pearson's linear correlation coefficient and *P* value between body kinematic variables and the changes of wing kinematic variables.

Movie S1. High-speed video recordings of an example pitch-dominated landing (PD) shown in Fig. 1D.

Movie S2. High-speed video recordings of an example roll-dominated landing (RD) shown in Fig. 1E.

Movie S3. High-speed video recordings of an example longitudinal-body-swing-dominated landing (SLon) shown in Fig. 1F.

Movie S4. High-speed video recordings of an example lateral-body-swing-dominated landing (SLat).

Movie S5. High-speed video recordings of an example pitch-roll combined landing (PR).

Movie S6. High-speed video recordings of an example landing with ceiling groping (CG).

Movie S7. High-speed video recordings of an example failed landing due to early body rotation (FER) shown in Fig. S2A.

Movie S8. High-speed video recordings of an example failed landing due to low body inversion with delayed leg extension (FDE) shown in Fig. S2B.

Movie S9. High-speed video recordings of an example failed landing due to low body inversion with minor body rotation (FMR).

References (*51*, *52*)

View/request a protocol for this paper from *Bio-protocol*.

REFERENCES AND NOTES

1. F. T. Muijres, M. J. Elzinga, J. M. Melis, M. H. Dickinson, Flies evade looming targets by executing rapid visually directed banked turns. *Science* **344**, 172–177 (2014).
2. T. Beatus, J. M. Guckenheimer, I. Cohen, Controlling roll perturbations in fruit flies. *J. R. Soc. Interface* **12**, 20150075 (2015).
3. R. C. Wilkerson, J. F. Butler, The Immelmann Turn, a pursuit maneuver used by hovering male Hybomitra hinei wrighti (Diptera: Tabanidae). *Ann. Entomol. Soc. Am.* **77**, 293–295 (1984).
4. W. G. Hyzer, Flight behavior of a fly alighting on a ceiling. *Science* **137**, 609–610 (1962).
5. M. Kovac, Learning from nature how to land aerial robots. *Science* **352**, 895–896 (2016).
6. K. Jayaram, J.-M. Mongeau, A. Mohapatra, P. Birkmeyer, R. S. Fearing, R. J. Full, Transition by head-on collision: Mechanically mediated manoeuvres in cockroaches and small robots. *J. R. Soc. Interface* **15**, 20170664 (2018).
7. C. Shen, M. Sun, Wing and body kinematics measurement and force analyses of landing in fruit flies. *Bioinspir. Biomim.* **13**, 016004 (2018).
8. F. Van Breugel, M. H. Dickinson, The visual control of landing and obstacle avoidance in the fruit fly Drosophila melanogaster. *J. Exp. Biol.* **215**, 1783–1798 (2012).
9. S. P. Sane, S. Balebail, S. K. Raja, Visual control of landing maneuvers in houseflies on vertical and inverted surfaces. *bioRxiv* 10.1101/448472 (2018).
10. S. Dalton, J. Kings, *Borne On The Wind: The Extraordinary World Of Insects In Flight* (1975).
11. S. N. Gorb, Uncovering insect stickiness: Structure and properties of hairy attachment devices. *Am. Entomologist* **51**, 31–35 (2005).
12. A. Borst, How do flies land? *Bioscience* **40**, 292–299 (1990).
13. A. Borst, Time course of the houseflies' landing response. *Biol. Cybern.* **54**, 379–383 (1986).
14. H. Wagner, Flow-field variables trigger landing in flies. *Nature* **297**, 147–148 (1982).
15. B. Cheng, B. W. Tobalske, D. R. Powers, T. L. Hedrick, Y. Wang, S. M. Wethington, G. T.-C. Chiu, X. Deng, Flight mechanics and control of escape manoeuvres in hummingbirds. II. Aerodynamic force production, flight control and performance limitations. *J. Exp. Biol.* **219**, 3532–3543 (2016).
16. W. R. Roderick, M. R. Cutkosky, D. Lentink, Touchdown to take-off: At the interface of flight and surface locomotion. *Interface Focus* **7**, 20160094 (2017).
17. M. V. Srinivasan, S.-W. Zhang, J. S. Chahl, E. Barth, S. Venkatesh, How honeybees make grazing landings on flat surfaces. *Biol. Cybern.* **83**, 171–183 (2000).
18. D. N. Lee, A theory of visual control of braking based on information about time-to-collision. *Perception* **5**, 437–459 (1976).
19. E. Baird, N. Boeddeker, M. R. Ibbotson, M. V. Srinivasan, A universal strategy for visually guided landing. *Proc. Natl. Acad. Sci.* **110**, 18686–18691 (2013).
20. M. Srinivasan, How insects infer range from visual motion. *Rev. Oculomot. Res.* **5**, 139 (1993).
21. T. Collett, Depth vision in animals. *Analysis of visual behavior* 111–176 (1982).
22. S. B. Fuller, A. D. Straw, M. Y. Peek, R. M. Murray, M. H. Dickinson, Flying Drosophila stabilize their vision-based velocity controller by sensing wind with their antennae. *Proc. Natl. Acad. Sci.* **111**, E1182–E1191 (2014).
23. J.-M. Mongeau, M. A. Frye, Drosophila spatiotemporally integrates visual signals to control saccades. *Curr. Biol.* **27**, 2901–2914. e2 (2017).
24. J. C. Theobald, D. L. Ringach, M. A. Frye, Dynamics of optomotor responses in Drosophila to perturbations in optic flow. *J. Exp. Biol.* **213**, 1366–1375 (2010).
25. T. Lindsay, A. Sustar, M. Dickinson, The function and organization of the motor system controlling flight maneuvers in flies. *Curr. Biol.* **27**, 345–358 (2017).
26. M. H. Dickinson, The initiation and control of rapid flight maneuvers in fruit flies. *Integr. Comp. Biol.* **45**, 274–281 (2005).
27. B. Cheng, B. W. Tobalske, D. R. Powers, T. L. Hedrick, S. M. Wethington, G. T. Chiu, X. Deng, Flight mechanics and control of escape manoeuvres in hummingbirds. I. Flight kinematics. *J. Exp. Biol.* **219**, 3518–3531 (2016).
28. B. Cheng, X. Deng, T. L. Hedrick, The mechanics and control of pitching manoeuvres in a freely flying hawkmoth (Manduca sexta). *J. Exp. Biol.* **214**, 4092–4106 (2011).
29. G. K. Taylor, H. G. Krapp, S. J. Simpson, Sensory systems and flight stability: What do insects measure and why? *Adv. In Insect Phys.* **34**, 231–316 (2007).
30. C. R. von Reyn, A. Nern, W. R. Williamson, P. Breads, M. Wu, S. Namiki, G. M. Card, Feature integration drives probabilistic behavior in the Drosophila escape response. *Neuron* **94**, 1190–1204.e6 (2017).
31. M. Sun, Insect flight dynamics: Stability and control. *Rev. Mod. Phys.* **86**, 615–646 (2014).
32. B. Liang, M. Sun, Nonlinear flight dynamics and stability of hovering model insects. *J. R. Soc. Interface* **10**, 20130269 (2013).
33. Y. Xiong, M. Sun, Dynamic flight stability of a bumblebee in forward flight. *Acta Mech. Sin.* **24**, 25–36 (2008).
34. M. J. Elzinga, F. van Breugel, M. H. Dickinson, Strategies for the stabilization of longitudinal forward flapping flight revealed using a dynamically-scaled robotic fly. *Bioinspir. Biomim.* **9**, 025001 (2014).
35. M. Sun, Y. Xiong, Dynamic flight stability of a hovering bumblebee. *J. Exp. Biol.* **208**, 447–459 (2005).
36. L. Ristroph, G. Ristroph, S. Morozova, A. J. Bergou, S. Chang, J. Guckenheimer, Z. J. Wang, I. Cohen, Active and passive stabilization of body pitch in insect flight. *J. R. Soc. Interface* **10**, 20130237 (2013).

37. I. Faruque, J. Sean Humbert, Dipteran insect flight dynamics. Part 1 Longitudinal motion about hover. *J. Theor. Biol.* **264**, 538–552 (2010).
38. B. Cheng, X. Deng, Translational and rotational damping of flapping flight and its dynamics and stability at hovering. *IEEE Trans. Robot.* **27**, 849–864 (2011).
39. M. Sun, J. K. Wang, Flight stabilization control of a hovering model insect. *J. Exp. Biol.* **210**, 2714–2722 (2007).
40. A. Borst, S. Bahde, What kind of movement detector is triggering the landing response of the housefly? *Biol. Cybern.* **55**, 59–69 (1986).
41. H. Eckert, K. Hamdorf, Excitatory and inhibitory response components in the landing response of the blowfly, Calliphora erythrocephala. *J. Comp. Physiol.* **138**, 253–264 (1980).
42. J. M. Ache, S. Namiki, A. Lee, K. Branson, G. M. Card, State-dependent decoupling of sensory and motor circuits underlies behavioral flexibility in Drosophila. *Nat. Neurosci.* **22**, 1132–1139 (2019).
43. E. Ilg, N. Mayer, T. Saikia, M. Keuper, A. Dosovitskiy, T. Brox, Flownet 2.0: Evolution of optical flow estimation with deep networks, in *Proceedings of the IEEE Conference on Computer Vision and Pattern Recognition* (2017), pp 2462–2470.
44. T. Kroeger, R. Timofte, D. Dai, L. Van Gool, Fast optical flow using dense inverse search, in *European Conference on Computer Vision* (Springer, 2016), pp 471–488.
45. L. Carlone, S. Karaman, Attention and anticipation in fast visual-inertial navigation. *IEEE Trans. Robot.* **35**, 1–20 (2019).
46. A. Suleiman, Z. Zhang, L. Carlone, S. Karaman, V. Sze, Navion: A 2-mW fully integrated real-time visual-inertial odometry accelerator for autonomous navigation of nano drones. *IEEE J. Solid-State Circuits* **54**, 1106–1119 (2019).
47. J. A. Faber, A. F. Arrieta, A. R. Studart, Bioinspired spring origami. *Science* **359**, 1386–1391 (2018).
48. C. Coulais, A. Sabbadini, F. Vink, M. van Hecke, Multi-step self-guided pathways for shape-changing metamaterials. *Nature* **561**, 512–515 (2018).
49. M. Stern, V. Jayaram, A. Murugan, Shaping the topology of folding pathways in mechanical systems. *Nat. Commun.* **9**, 4303 (2018).
50. J. M. Lee, *Riemannian manifolds: An introduction to curvature* (Springer Science & Business Media, 2006).
51. T. L. Hedrick, Software techniques for two- and three-dimensional kinematic measurements of biological and biomimetic systems. *Bioinspir. Biomim.* **3**, 034001 (2008).
52. R. M. Murray, Z. Li, S. S. Sastry, *A Mathematical Introduction to Robotic Manipulation* (CRC, 1994).

Acknowledgments: We thank X. Wang and D. Yeung for assistance with the high-speed video recordings, digitizing landing kinematics, and data analyses. **Funding:** This research was supported by the National Science Foundation (CMMI-1554429 and IIS-1815519 to B.C. and IIS-1815476 to J.Z.) and the Pennsylvania State University. **Author contributions:** P.L., B.C., and S.P.S. contributed to the design of the experiments; P.L. and B.C. performed the experiments; P.L. analyzed the data; P.L., B.C., S.P.S., J.-M.M., and J.Z. contributed to the interpretation of findings and the preparation of the manuscript. **Competing interests:** The authors declare that they have no financial or other competing interests. **Data and materials availability:** All data needed to evaluate the conclusions in the paper are present in the paper and/or the Supplementary Materials. Additional data related to this paper may be requested from the authors.

Submitted 28 February 2019
Accepted 14 September 2019
Published 23 October 2019
10.1126/sciadv.aax1877

Citation: P. Liu, S. P. Sane, J.-M. Mongeau, J. Zhao, B. Cheng, Flies land upside down on a ceiling using rapid visually mediated rotational maneuvers. *Sci. Adv.* **5**, eaax1877 (2019).